Special Issue: Balkantrib 2020

Institution of MECHANICAL ENGINEERS
Journal of ENGINEERING TRIBOLOGY

Proc IMechE Part J:
J Engineering Tribology
1–12

DOI: 10.1177/13506501211062522
journals.sagepub.com/home/pij
SAGE

Pulsed plasma nitriding of high velocity oxy-fuel sprayed Inconel 625 coatings

Harun Mindivan

Abstract

A hardening of high velocity oxy-fuel sprayed Inconel 625 coating systems was performed by pulsed plasma nitriding treatment. After deposition of an Inconel 625 coating, samples were pulsed plasma nitrided at 520 °C for 12 h in a gas ratio of 3:1 N_2 and H_2 under a constant pressure of 2.5×10^2 Pa. Pulsed plasma nitriding improved the microhardness of the high velocity oxy-fuel sprayed Inconel 625 coating from 355 to 401 $HV_{0.05}$. The high velocity oxy-fuel-sprayed Inconel 625 coating after pulsed plasma nitriding process showed excellent corrosion resistance as well as a reduction of both the friction coefficient and wear rate during the sliding phase in a 3.5 wt.% NaCl solution against sliding action of Al_2O_3 ball.

Keywords

Corrosion, pulsed plasma nitriding, high velocity oxy-fuel spraying, Inconel 625, tribocorrosion

Date received: 17 June 2021; accepted: 5 November 2021

Introduction

Thermally sprayed Inconel 625 coatings on steel substrates exhibit excellent corrosion, corrosion-wear, and erosion-corrosion resistance in harsh operating conditions, since nickel-based coatings are electrochemically nobler than ordinary steel substrates.[1–3] Because of the high cost of the components of Inconel 625 on a large scale, these excellent properties have positioned them as the top coating layer for the protection of submerged components.[4] However, Inconel 625 coatings prepared by thermal spraying might not be suitable to protect the surface in hostile environments because of the presence of pores, micro-cracks, gaps and oxide inclusions at inter-splat boundaries and the localized attacks between resolidified regions and unmelted particles.[3] Generally, the performance and the service life of coatings increase with their density and cohesive strength. Due to the severe impact of particles sprayed under a condition of high velocity and low temperature, high velocity oxy-fuel (HVOF) coatings offer low porosity, low surface roughness, high bonding strength and high hardness compare to other coating technique.[5–8] Chen et al. (2019) studied the tribological behavior of various Inconel 625 coatings obtained through flame spraying (F), arc spraying (A), plasma spraying (P), or HVOF spraying (H) in a saline solution and deionized water. Their results indicate that the corrosion-wear resistance of the Inconel 625 coatings was in the order F > A>P > H due to the high oxide content within its coating layer as an antiwear phase for tribocorrosion protection. Post-coating treatments can be a potential way to remove some of defects or surface transformations that are detrimental to the tribocorrosion performance of coatings. Liu et al. (2007) improved the corrosion and wear resistance of the HVOF-sprayed Inconel 625 and WC-based coatings by laser treatment, which was achieved by removing the discrete splat structure, porosity, microcrevice and lowering microgalvanic activity between the coating and the matrix.[9] It is reported that the wear and corrosion resistance of the HVOF-sprayed coatings could be further increased by plasma nitriding.[10,11]

Plasma nitriding is a modern technique for surface hardening of metallic components to accomplish the improvement in mechanical properties and wear and corrosion resistance of Ni and Fe based alloys, because it has excellent dimensional control, short cycle time, low distortion, environment friendliness, ease of selective nitriding, low process gas consumption and automation.[12] It is a thermochemical process used to achieve surface hardening by the diffusion of the nitrogen element into the surface of metals.[13] One of the difficulties faced during traditional nitriding of thermal sprayed coatings is its sensitivity to temperature in the conventional plasma

Department of Mechanical Engineering, Bilecik Şeyh Edebali University, Turkey

Corresponding author:
Harun Mindivan, Department of Mechanical Engineering, Bilecik Şeyh Edebali University, Bilecik, Turkey.
Email: hmindivan@gmail.com

nitriding process because the work piece is the plasma cathode itself.[12] Pulse plasma technology, employing pulse duration and duty cycle control, ensures a more uniform temperature distribution in the thermal sprayed coating systems and at the same time, allows the use of higher plasma power without the risk of overheating the surface.[14] Pulsed plasma nitriding (PPN) process, promoting a shorter time in the same nitriding depths,[15] could be considered as an appropriate candidate for post-deposition treatment compared to the other types of nitriding treatments.[10,11]

In general, thermochemical processes are applied to bulk materials. Nevertheless, some researchers have combined the processes of thermal spray with other surface thermochemical treatments, and proved the feasibility of HVOF sprayed stainless steel[10,11] and Inconel 625[8] coatings using various industrial surface hardening processes. Also, avoiding a phase transformation of the bulk and/or coating during the nitriding process offers a significant advantage because it minimizes the distortions that arise from the boriding and carburizing of the coating in the as-sprayed condition. The minor probability of surface distortion and dimensional variations makes it possible to reduce or even to eliminate the need for subsequent expensive finishing processes before the coating is put into service. On the other hand, the plasma nitrided Inconel 625 alloy under glow discharge conditions shows a diffusion-type chromium nitride layer, which results in an enhancement of the corrosion, frictional resistance and fatigue strength of the bulk alloy.[13] Varela et al.[16] studied the microabrasive wear of plasma nitrided Inconel 625 alloy using a micro-scale abrasion tester with free ball configuration. The authors reported that the formation of a nitride layer consisting of nitrogen expanded face-centered cubic (fcc) phase (γ_N) and CrN nitride improves the wear resistance and promotes hardening due to the higher compressive residual stresses. The current study investigates the possibility of PPN of HVOF-sprayed Inconel 625 coatings. In the present work, Inconel 625 was coated on a low carbon steel substrate using a HVOF coating process and then pulsed plasma nitrided at 520 °C for 12 h in a gas ratio of 3:1 N_2 and H_2 under a constant pressure of 2.5×10^2 Pa. Characterizations of the coatings were carried out by using X-ray diffraction (XRD), light optic microscope (LOM), scanning electron microscope (SEM), and microhardness measurements. The corrosion behavior of the coatings was evaluated using a three-electrode cell, and the tribocorrosion assessment was carried out using a reciprocating ball-on-plate tribometer in which the tribological contact was immersed in the 3.5 wt.% NaCl solution.

Table 1. The nominal composition of the Inconel 625 powder used during HVOF spraying (wt.%).

Feedstock powder	C	Mn	Si	Cr	Mo	Ni	Fe	Nb
Inconel 625	0.025	0.2	0.4	22	9	Balance	3.0	3.5

Materials and methods

In this study, St37 low-carbon steel plates as the base metal were cut to the dimensions of $100 \times 50 \times 4$ mm^3 (length × width × thickness). The chemical compositions of the St37 low-carbon substrate were 0.11% C, 0.44% Mn, 0.03% W, 0.18% Si, 0.012% P, and 0.01% S. Prior to the spraying process, the steel plates were sand-blasted to remove any dust or impurities, and to provide the substrate with proper roughness to increase the coating bonding strength to the substrate. In this study, commercially available Inconel 625 feedstock in the form of powder (−45 to +11 μm) was used for the HVOF technique. The chemical composition of the coating powder is given in Table 1. The process parameters for HVOF spraying are given in Table 2. Before PPN, the surfaces of the HVOF sprayed Inconel 625 coating were grinded using 1200 grit SiC paper and polished up to 1 μm particle size using an Al_2O_3 suspension to achieve a certain surface uniformity. At this stage, it was observed that the coating surface had a roughness of approximately 0.08 μm. Finally, the surfaces were ultrasonically cleaned in an acetone bath for 10 min. The coatings were then pulsed plasma nitrided at 520 °C for 12 h under a constant pressure of 2.5×10^2 Pa in an industrial furnace (Er-Mir Textile and Machine Ltd) in a gas ratio of 3:1 N_2 and H_2. Cross-sections of the coatings were prepared by using SiC papers and Al_2O_3 suspension down to 1 μm particle size for metallographic and microhardness examinations.

Microstructural characterization of the coatings was made by microscopic examinations, XRD and microhardness measurements. Microscopic examinations were performed on the cross-sections of the coatings by utilizing Nikon Eclipse LV150 LOM and a Zeiss Supra field emission gun scanning electron microscope (FEG-SEM) equipped with energy dispersive X-ray spectroscopy (EDS). XRD analysis was carried out by utilizing CuK_α radiation with a Panalytical Empyrean diffractometer. The cross-sectional microhardness measurements were carried out using a Vickers microhardness tester (Shimadzu HVM) with a load 50 g and a dwell time of 15 s.

Corrosion tests were carried out using PCI4/750 Gamry potentiostat/galvanostat controlled by a computer

Table 2. Process parameters of HVOF thermal spray.

Oxygen pressure (kPa)	1034
Fuel pressure (kPa)	620
Air pressure (kPa)	724
Powder feed rate (m^3/h)	0.81
Spray rate (kg/h)	6.35
Spray distance (m)	0.28

with DC105 corrosion analysis software. The embedded coatings in epoxy resin were utilized as working electrodes. The Ag/AgCl was the reference electrode and the platinum wire was the counter electrode. Experiments were performed at room temperature in a glass cell containing 3.5 wt.% NaCl solution. Prior to the corrosion tests, all the coatings were polished with 1 µm particle size using an Al_2O_3 suspension. Before potentiodynamic polarization measurements, an initial delay of 30 min was employed in order to measure the open circuit potential (OCP) between working and reference electrodes. Potentiodynamic polarization curves were generated by sweeping the potential from cathodic to anodic direction at a constant scan rate of 1 mVs^{-1}, starting from −0.8 up to −0.2 V. The corrosion tests were evaluated from the potentiodynamic polarization. Finally, the corroded surfaces were analyzed by FEG-SEM/EDS in order to identify the morphologies of the corrosion surfaces. Corrosion rates were then calculated in millimeter/year (mmpy) using equation (1):

$$\mathrm{CR} = \frac{I_{corr}.K.EW}{d.A} \quad (1)$$

where: CR is the corrosion rate; I_{corr} is the corrosion current (amps); K is a constant value (3272); EW is the equivalent weight (g/equiv), d represents material density (g/cm^3); A is the nominal surface area (cm^2).

Tribocorrosion tests were conducted in a three-electrode-chemical cell containing 25 ml of 3.5 wt.% NaCl solution installed on a linear reciprocating ball-on-plate configuration. Tests were performed under a load of 5 N, a stroke length of 11.5 mm, a speed of 1.9 cm s^{-1}, and a total sliding distance of 57.5 m. During the test, an exposure area of ∼2.5 cm^2 was exposed to the corrosive electrolyte. Ponthiaux et al.[17] reported that the analysis of OCP transients obtained under potentiostatic conditions provides information on the degradation of the passive film (cracking or spalling) and on the kinetics of the restoration of the passive film. Papageorgiou et al.[18] carried out under OCP to simulate better the offshore working conditions of the Inconel 625 alloy in 3.4 wt.% NaCl. Therefore, reciprocating sliding tests were carried out under OCP conditions. The OCP was recorded before, during and after reciprocation sliding contact with a 10 mm diameter Al_2O_3 ball (9.56 GPa) with surface roughness (R_a) of 0.01 µm. The tribocorrosion tests consisted of the three steps: (1) OCP stabilization for 600 s before sliding; (2) OCP variation for 2700 s during sliding; (3) OCP stabilization for 600 s after sliding. All tribocorrosion tests were repeated at least two times, and the results were averaged to obtain the average wear rate. Width and depth of the wear tracks were measured by a surface profilometer (Mitutoyo Surftest SJ-400) to calculate wear rate of the coatings.

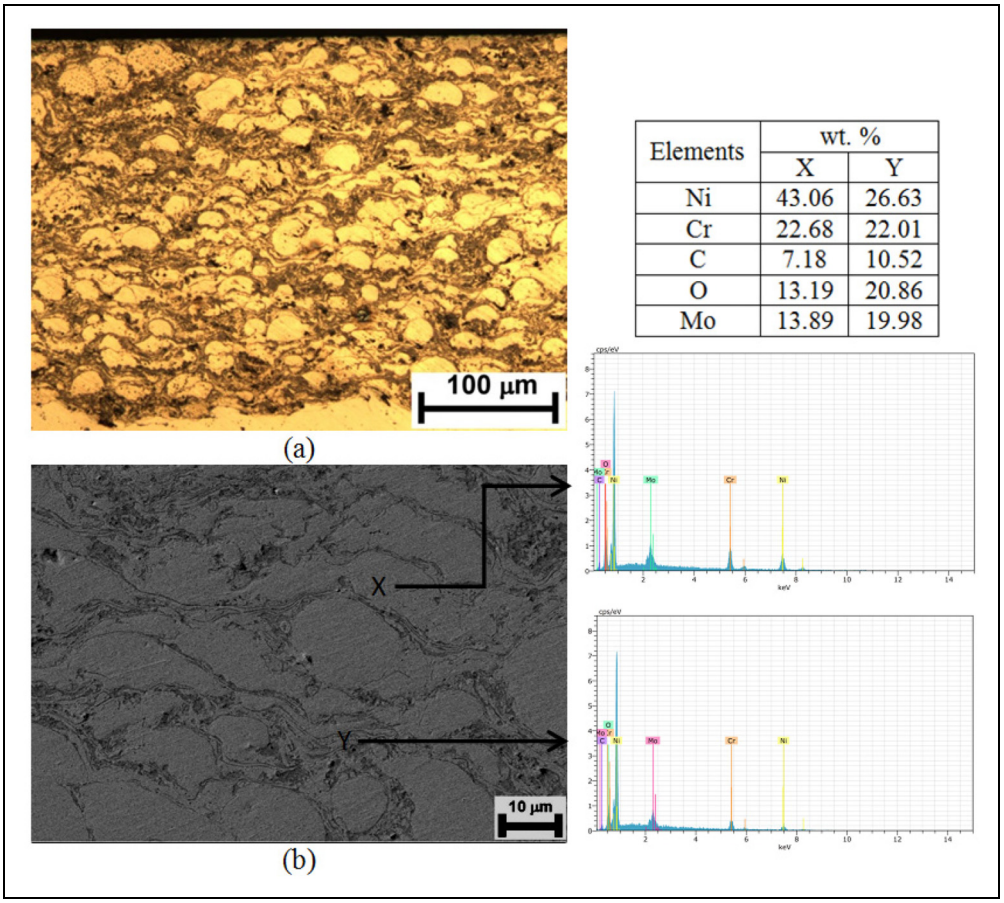

Figure 1. (a) LOM cross-section and (b) SEM micrographs and EDS results of HVOF-sprayed Inconel 625 coating.

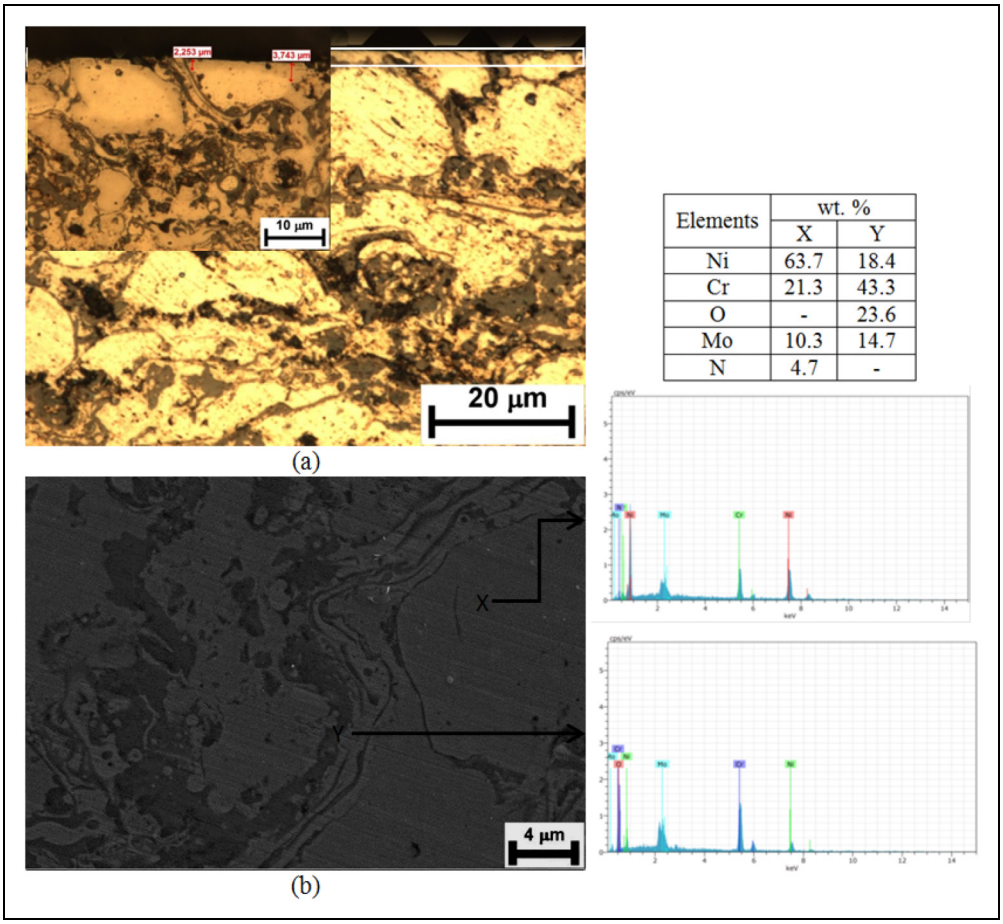

Elements	wt. %	
	X	Y
Ni	63.7	18.4
Cr	21.3	43.3
O	-	23.6
Mo	10.3	14.7
N	4.7	-

Figure 2. (a) Low and high magnification LOM cross-section and (b) SEM surface micrographs of nitriding coating after PPN process.

The wear rate (W_R) is calculated as the volume worn per unit load per unit distance and its calculation formula is as follows:

$$W_R = \frac{V}{F.S} \tag{2}$$

where V is the total wear volume loss in mm^3, F and S are the applied load in N and total sliding distance in m, respectively. After sliding tests, coatings are ultrasonically cleaned in acetone. The coefficient of friction (COF) curves were recorded automatically using a computer connected with the tribometer. After tribocorrosion tests, the worn surfaces of the wear tracks that formed on the examined coatings were investigated by the FEG-SEM.

Results and discussions

Figure 1 displays the cross-section microstructure of Inconel 625 coating examined using the LOM and SEM. The as-sprayed coating had a thickness of 350 µm (Figure 1(a)). The LOM and SEM images show a characteristic thermally sprayed microstructure.[3,8] In the as-sprayed condition, the coating is built up from the successive impacts of individual particles that are heated and accelerated towards the substrate by the spraying process (Figure 1(b)). On arrival at the steel substrate the particles are fully or partially molten. On impact molten material spreads out and resolidifies whereas non-molten material deforms and adheres mainly by mechanical interlocking. Individual particles, or splats, can be seen, it is also clear that the coating shown in Figure 1(b) consists of two distinct types of material: deformed, near-spherical particles as well as lamellar splat-like features. The lamella type microstructure with oxide strings aligned parallel to the steel surface is characteristic of coatings produced by HVOF process as reported by Fantozzi et al.[2] The coating presents a compact coating layer with small defects of spherical morphology in the inner parts of splats and the network of inter splat linear defects formed on the splat boundaries during deposition. EDS analysis shows that the Inconel 625 coatings were composed of nickel, chromium, carbon, oxygen and molybdenum. As emerges from the EDS analysis in Figure 1(b), the brighter areas (X region) were depleted in molybdenum, oxygen and enriched in nickel, but the splat boundaries (Y region) of HVOF coating were rich in chromium oxides containing traces of molybdenum oxides and poor in nickel. The carbon contamination may arise from the propane fuel gas used in the HVOF spray system.

Figure 2 shows the LOM cross-section and SEM surface micrographs of the nitriding coating. As can be seen in the LOM images of Figure 2(a), PPN process

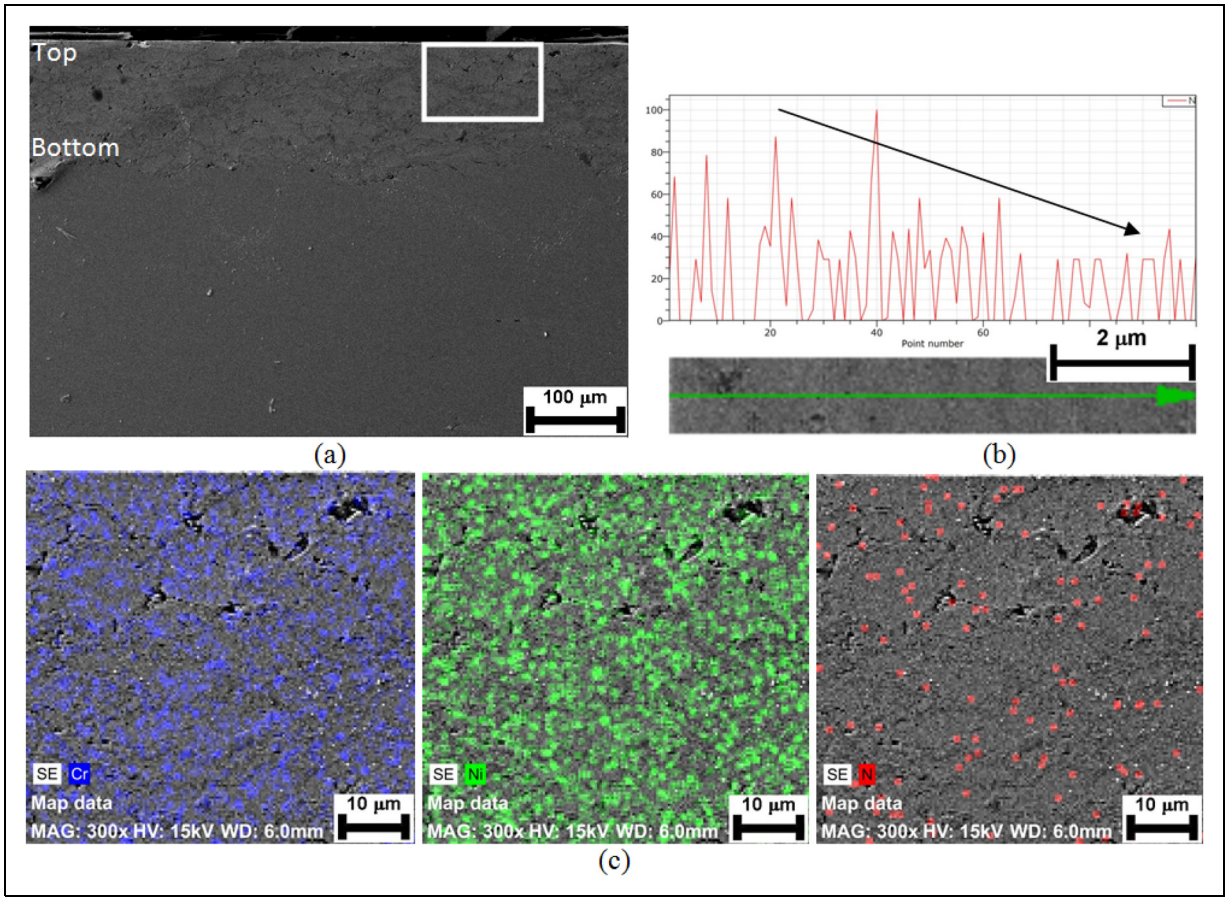

Figure 3. (a) SEM cross-section micrograph, (b) nitrogen depth concentration and (c) elemental concentration of chromium, nickel and nitrogen in the nitriding coating.

produced a relatively thin nitrided layer (~5 µm). According to the research by Park et al., the HVOF-sprayed 316 and 410 stainless steel coatings had the thinnest and thickest nitride layers, respectively.[19] Microstructural components were determined by performing EDS analysis on the surface of the HVOF-sprayed Inconel 625 coating after PPN process. As can be seen from Figure 2(b), the brighter area consists of nickel, chromium, molybdenum and nitrogen elements, while the splat boundaries compose of chromium, oxygen, nickel and molybdenum. The oxidized regions also appeared to have low nickel content. According to the

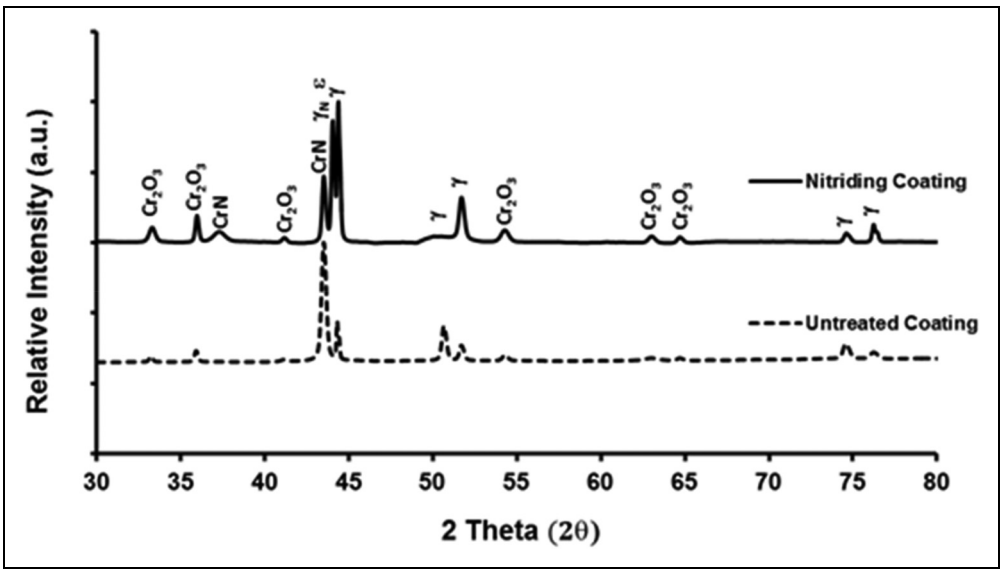

Figure 4. XRD patterns of HVOF-sprayed Inconel 625 coating before and after PPN process.

Table 3. Surface roughness (R_a, R_y, R_z, R_q) and hardness values of the coatings.

	Surface roughness values				
Surface	R_a	R_y	R_z	R_q	Hardness $HV_{0.05}$
Untreated coating	0.08	1.3	1.0	0.12	355 ± 26
Nitriding coating	0.08	1.1	0.9	0.11	401 ± 54

EDS results, there were no diffusion areas of nitrogen in the splat boundaries and the EDS experiment confirmed existence of the higher amount of chromium and oxygen in splat boundaries in agreement with Park et al.[19] The results are due to the chromium oxides formed in the oxygen rich area. In the HVOF process, it is possible that the inter-splat oxide is formed via in-flight oxidation. Therefore, it was recognized that formation of dense oxides acting as a barrier at the splat boundaries affected the nitrogen diffusion significantly. EDS line scan and corresponding elemental mapping recorded with EDS in Figure 3 were carried out. It shows that the nitrogen concentration, obtained at the red line, gradually changed in the thickness of the nitriding coating from the top to the bottom of the coating (Figure 3(b)). The EDS mapping clearly indicates better concentrations of chromium, nickel and nitrogen in the nitriding coating (Figure 3(c)).

The XRD patterns of the coatings are shown in Figure 4. The coatings gave major peaks which could be identified as belonging to a fcc nickel based matrix (γ) and additional minor peaks that corresponded to the Cr_2O_3 phase, but some extra peaks can be seen in the ones obtained for nitriding coating. A mix peak of ϵ-Fe_{2-3N} phase with fcc (γ) phase at the 2θ position of 43° and chromium nitride (CrN) phase at the position of 2θ angles of 36.7°, 43.4°, and 64° were observed in the nitriding coating. The other additional peak was attributed to metastable fcc nitrogen solid solutions denoted γ_N. A recent work[20] reported that the broadening of nickel peaks is likely due to the deformation of the crystal structure due to the presence of nitrogen in solid solution during the nitriding process. Table 3 shows the results of the roughness and hardness values of the coatings. According to the surface roughness measurements, the surface quality and morphology did not changed after PPN treatment (Figure 5). On the other hand, microhardness measurements taken on the cross-section of the untreated and nitriding HVOF-sprayed Inconel 625 coatings indicate $355 \pm 26\ HV_{0.05}$ and $401 \pm 54\ HV_{0.05}$, respectively. Figure 3(b) shows the nitrogen depth concentration profile of the nitriding coating. The chemical nitrogen concentration-depth profile shows slightly decreasing nitrogen content (from 16 wt.% to 4.7 wt.%) up to a 5 μm. Beyond ~5.0 μm depth, the nitrogen content decreased to 0.0 wt.%, corresponding to the untreated HVOF-sprayed Inconel 625 coating core. Therefore, a large range of measured microhardness along the coating after PPN process is due to the change of the amount of nitrogen gradually along the coating (Figure 3(b)), accompanying the heterogeneous distribution of nitrogen due to the oxide lamellae as a barrier layer at the splat boundaries (Figure 2(b)). Microhardness profile in the nitriding HVOF-sprayed Inconel 625 coating is given in Figure 6.

In order to determine the effect of PPN process on corrosion behavior, the OCP plots for the untreated and nitriding HVOF-sprayed Inconel 625 coatings with time were obtained by electrochemical corrosion testing in 3.5 wt.% NaCl solution (Figure 7). The OCP value can be used to measure the corrosion tendency of the coating in an aqueous solution and a higher OCP value means lower corrosion tendency.[21] The OCP plots for the untreated HVOF-sprayed Inconel 625 coating shows potentials ranging between −518 and −566 mV, while for nitriding coating the potentials range from −414 mV and −496 mV. The results indicate that the PPN process results in increased corrosion resistance.

The potentiodynamic polarization curves (anodic and cathodic) as represented in Figure 8 demonstrate an increase in corrosion performance of HVOF-sprayed

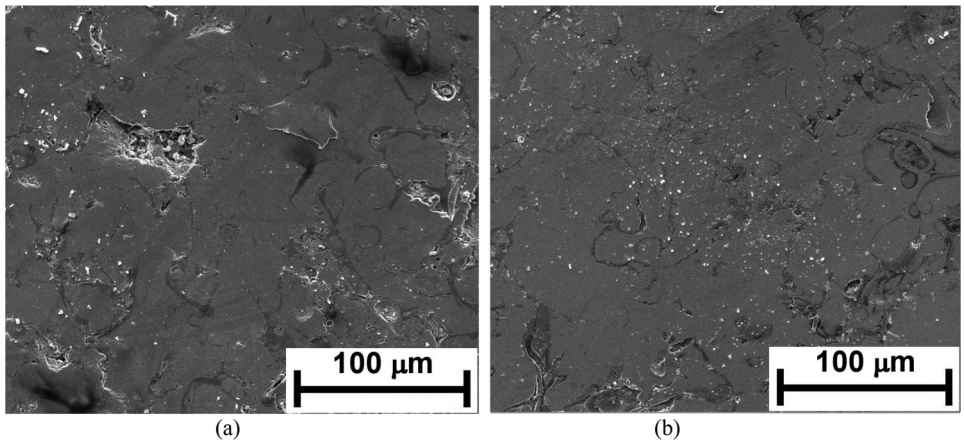

Figure 5. SEM surface micrographs of HVOF-sprayed Inconel 625 coating (a) before and (b) after PPN process.

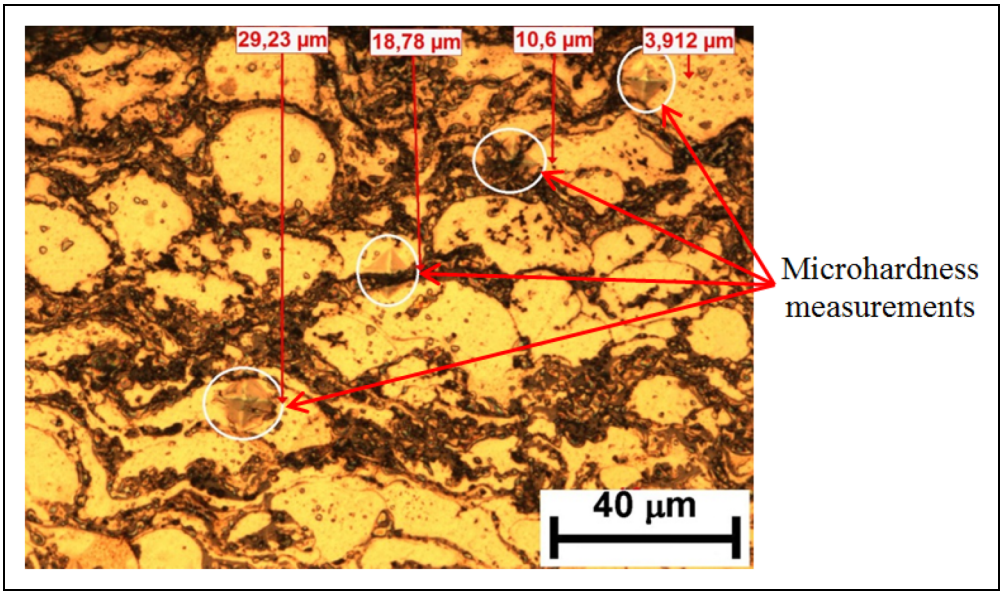

Figure 6. Microhardness profile measurements in the nitriding HVOF-sprayed Inconel 625 coating.

Inconel 625 coating by the PPN process as it indicated by increase in corrosion potential (from −575 mV to −506 mV), reduction in corrosion current (from 3.38×10^{-6} to 2.91×10^{-6} A/cm^2) and decrease in corrosion rate (from 11.95×10^{-3} to 10.28×10^{-3} mmpy). Nitriding coating corrodes at 14% slower rate when compared to the untreated HVOF-sprayed Inconel 625 coating. Nitrides such as ϵ-Fe_{2-3N} and CrN are noble phases and hence, they provide protection while remaining intact.[13,20,22]

Figure 9 shows the surface morphologies of the untreated and nitriding HVOF-sprayed Inconel 625 coatings which are immersed into chloride-containing solution. Corrosion test results showed no sign of corrosion attack on the nitriding coating (Figure 9(b)), whereas, a localized corrosion attack with pits up to ~2–3 µm wide on the regions between adjacent splats was observed on the untreated HVOF-sprayed Inconel 625 coating (Figure 7(a)). These regions have a complex heterogeneous microstructure (Figure 1) including a mixture of nonmelted and resolidified material and oxidized regions. Such mechanism has been described already by Neville and Hodgkiess.[23] The EDS element analyses of the spots marked X and Y shown in

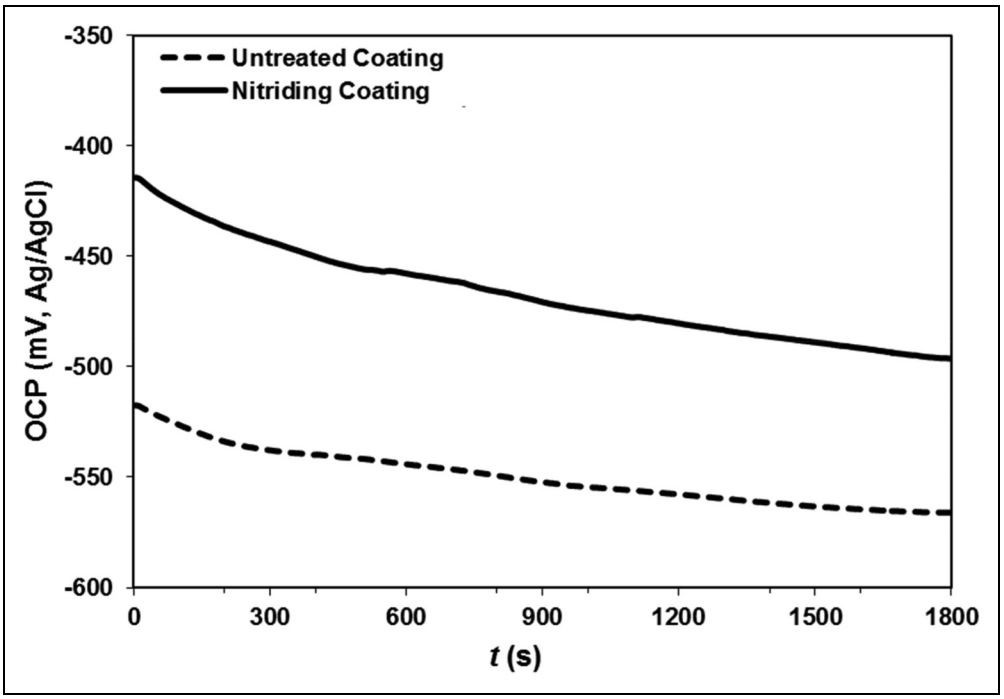

Figure 7. OCP plots for untreated and nitriding HVOF-sprayed Inconel 625 coatings recorded in 3.5 wt.% NaCl solution.

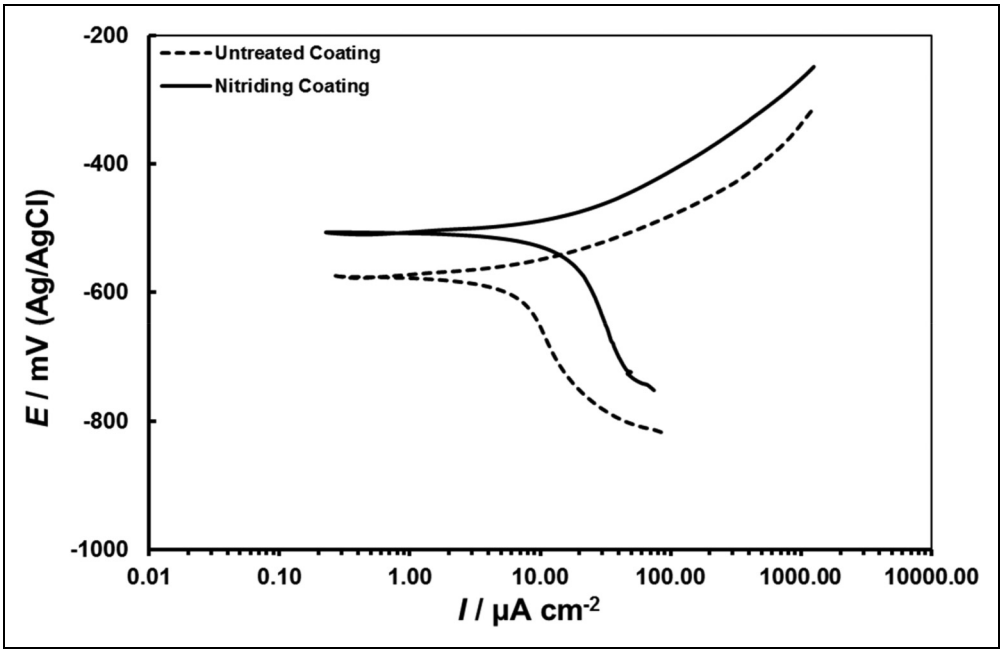

Figure 8. Potentiodynamic polarization curves of the untreated and nitriding HVOF-sprayed Inconel 625 coatings recorded in 3.5 wt.% NaCl solution.

Figure 9 showed a corrosion surface consisting of regions of varying chromium content. The penetration of corrosive medium through discrete splats in the coating would potentially lead to the attack of the coating and/or the substrate. There was a slight increase observed in the surface roughness of the untreated HVOF-sprayed

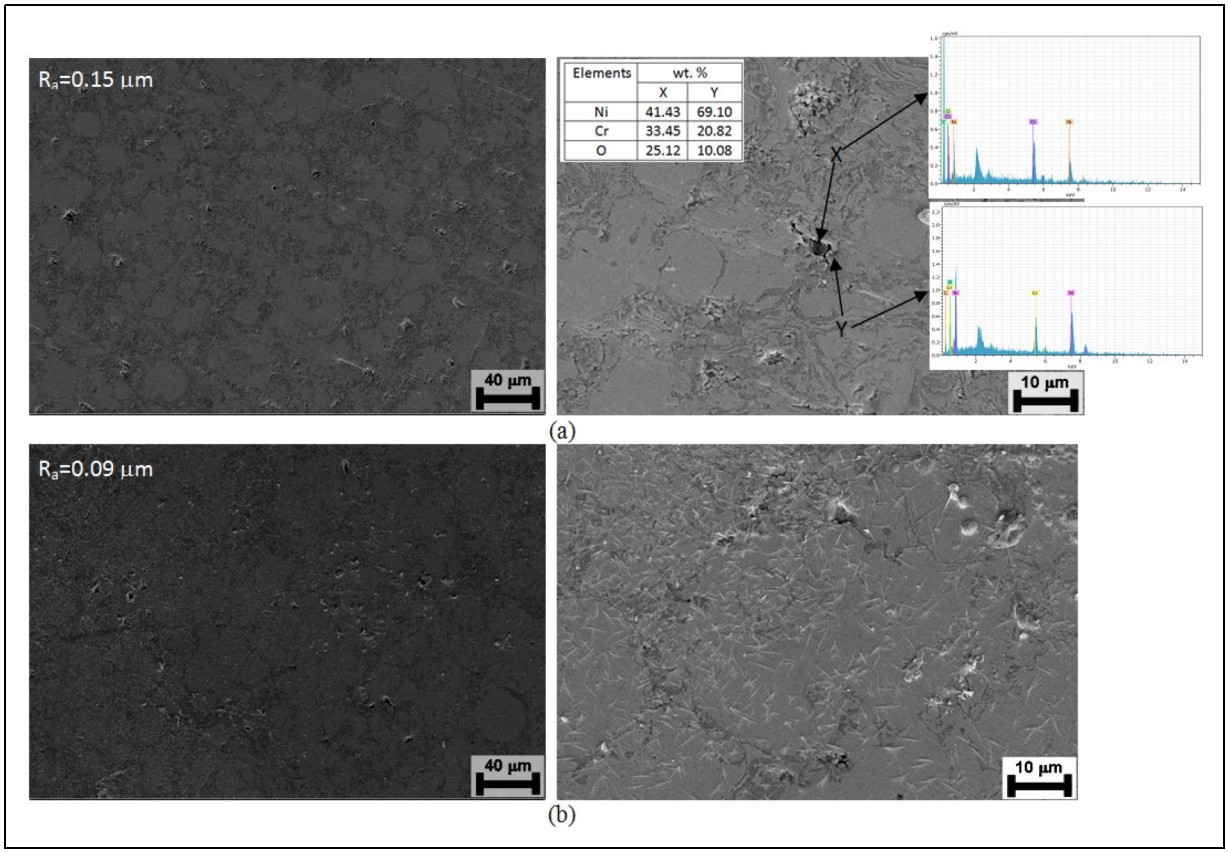

Figure 9. Low and high magnification SEM micrographs of the (a) untreated and (b) nitriding HVOF-sprayed Inconel 625 coatings after the corrosion tests.

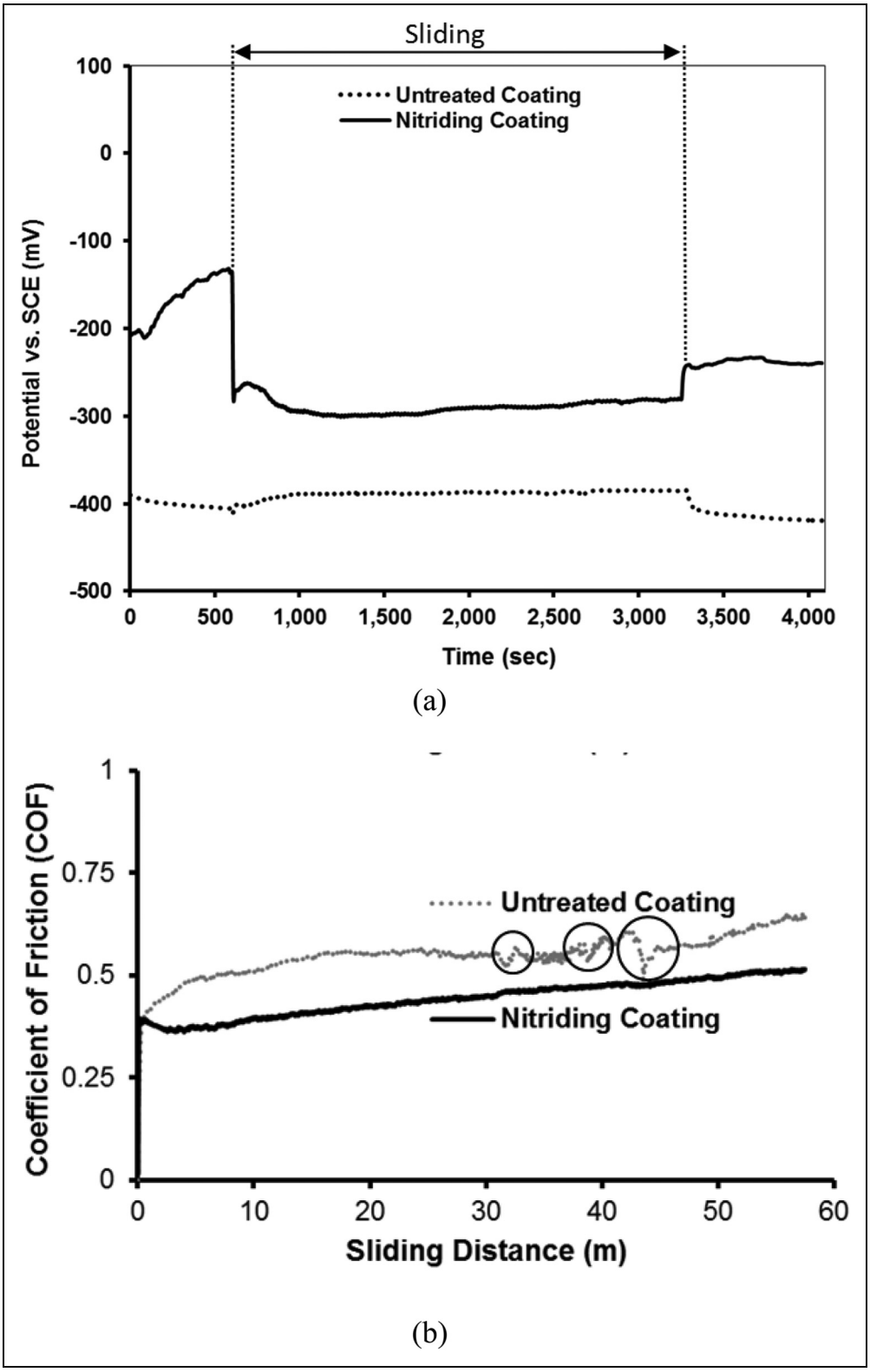

Figure 10. Evolution of the (a) OCP and (b) COF recorded in-situ before, during and after sliding in 3.5 wt.% NaCl solution.

Inconel 625 coating ($R_a = 0.15$ μm) at the end of the corrosion test compared to the start of the test ($R_a = 0.08$ μm). Slightly surface roughness in the untreated HVOF-sprayed Inconel 625 coating also means increased possibility for the accumulation of corrosion products. However, the nitriding coating remained largely unaffected in the same solution, despite the formation of surface patina, by the corrosion testing (Figure 9(b)).

The typical OCP and COF curves of the untreated and nitriding coatings during the tribocorrosion tests were showed in Figure 10. In generally, the value of OCP is a vital parameter to reflect the corrosion state of coating.

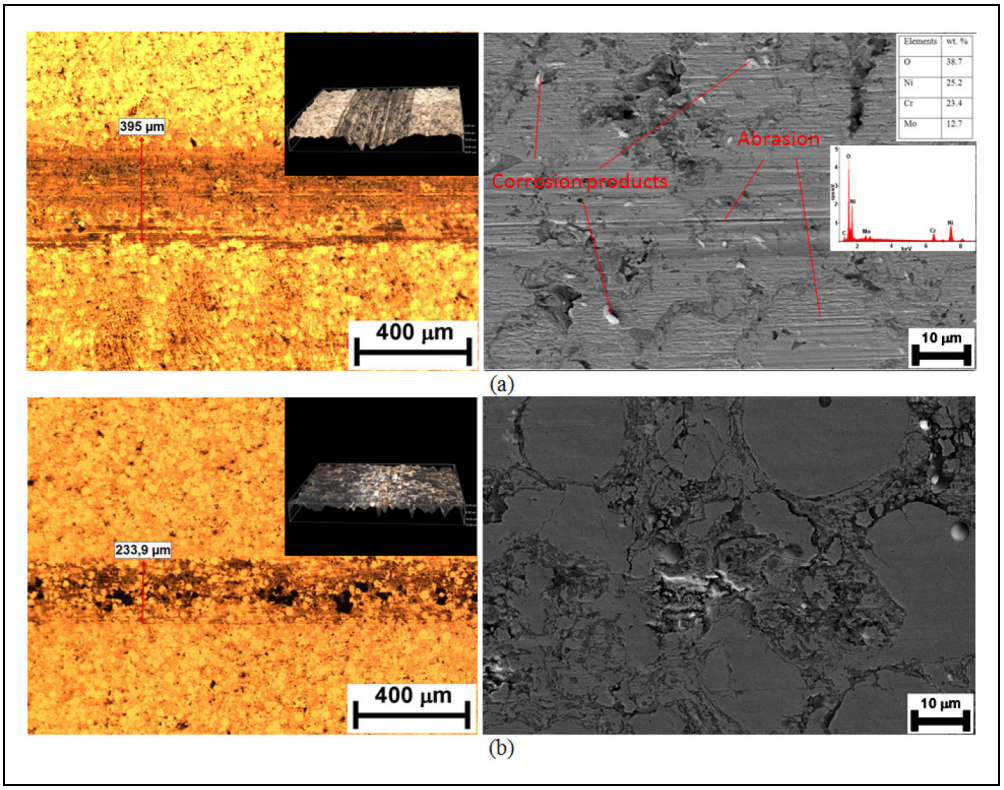

Figure 11. 3D Profiles, LOM and SEM images of the wear tracks of the (a) untreated and (b) nitriding HVOF-sprayed Inconel 625 coating in OCP conditions.

In the static state (the first 600 s), the OCP of the untreated coating was relatively stable with −405 mV, while for the nitriding coating; the OCP increased from −207 mV to −136 mV. When sliding started, it can be clearly seen that on the evolution of OCP for untreated coating, a slightly increase was observed on the onset of the sliding, followed by relatively stable values during sliding. After sliding, the values decreased rapidly near the initial values. In case of the nitriding coating, when sliding was initiated, a sudden drop in the potential of ∼140 mV can be observed. When sliding ceased, the potential increased again indicating a repassivation of the worn surface, showing slightly lower values in comparison with those before the wear test. Whether it is static or sliding, the potential of the nitriding coating was higher than that of the untreated coating, indicating that the PPN process was effective in protecting the HVOF-sprayed Inconel 625 coating from corrosion during sliding. The untreated coating exhibited the highest and most unstable friction with sudden fluctuations at certain time intervals (marked with circles), confirming its already known poor tribocorrosion characteristics, and thus the need for surface protective treatments. For the COF, it had been reported that the

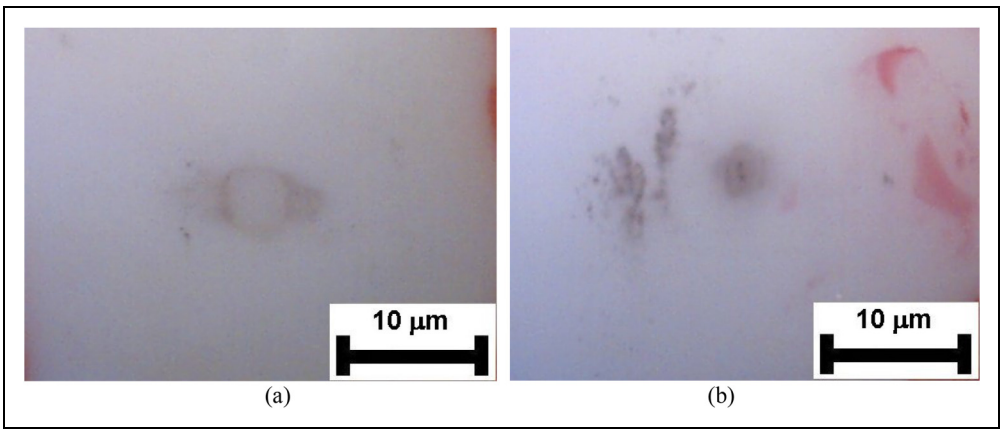

Figure 12. LOM images of the Al_2O_3 balls sliding against the (a) untreated and (b) nitriding HVOF-sprayed Inconel 625 coatings after tribocorrosion tests.

fluctuation of COF was closely related to the formation, oxidation and ejection of wear debris from the contact area.[24] The COF values for the nitriding coating were decreased during approximately first 1.7 m then continued to increase by approximately 0.51 till the end of the sliding. It can be clearly seen that the nitriding coating also showed a lower and more stable COF when compared with the untreated coating.

Figure 11 presents the 3D profiles, LOM and SEM images of the worn surfaces the untreated and nitriding coatings. From the 3D profiles and LOM images, a clear difference in the wear track size can be noticed, being considerably wider and deeper for the untreated coating. Parallel abrasion grooves were visible on the worn surface of untreated coating, and no smeared material was observed in the contact (Figure 11(a)). Some corrosion products can be observed in the track, formed as consequence of localized corrosion taking place in the worn surface. The EDS analysis revealed a considerable amount of oxygen along the whole wear track, which could be consequence of crushing and spreading of the oxidized detached material remaining in the tribological contact. On the other hand, the worn surface of the nitriding coating was much smoother and did not present signs of abrasive processes (Figure 11(b)). This was confirmed by the 3D profile measured by profilometry across the wear track. The wear rate of the nitriding coating (1.5×10^{-5} mm^3/Nm) was much lower compared with the untreated coating (0.63×10^{-5} mm^3/Nm), which is consistent with the combined results of electrochemical and friction coefficient measurements. No abrasion signs were observed in the Al_2O_3 balls indicating a negligible wear damage of the counter body as shown in Figure 12.

Conclusions

Corrosion and tribocorrosion tests were performed on a HVOF-sprayed Inconel 625 coating that was pulsed plasma nitrided at 520 °C for 12 h in a gas ratio of 3:1 N_2 and H_2 under a constant pressure of 2.5×10^2 Pa. For comparison the untreated HVOF-sprayed Inconel 625 coating was also investigated. Following conclusions could be drawn:

- The PPN process provided with nitrides such as ϵ-Fe_{2-3N} and CrN on the HVOF-sprayed Inconel 625 coating. After the PPN, the microhardness measured on the outer surface of HVOF-sprayed Inconel 625 coating increased from 355 ± 26 $HV_{0.05}$ to 401 ± 54 $HV_{0.05}$.
- The HVOF sprayed Inconel 625 coating after PPN process showed excellent corrosion resistance as well as a reduction of both the friction coefficient and wear rate during the sliding phase in a 3.5 wt.% NaCl solution against sliding action of Al_2O_3 ball.

Acknowledgments

The financial support of the research foundation of Bilecik Şeyh Edebali University (Project No.: 2019-02.BŞEÜ.03-01) is gratefully acknowledged. I would also like to express our thanks to Dr Ersin. E. KORKMAZ for the nitriding treatment applied to the samples. This paper has been presented at the 10th International Conference on Tribology – BALKANTRIB "20 organized in Belgrade, on May 20–22, 2021."

Declaration of Conflicting Interests

The author declared no potential conflicts of interest with respect to the research, authorship, and/or publication of this article.

Funding

The author received no financial support for the research, authorship, and/or publication of this article.

ORCID iD

Harun Mindivan https://orcid.org/0000-0003-3948-253X

References

1. Bolelli G, Lusvarghi L and Giovanardi R. A comparison between the corrosion resistances of some HVOF-sprayed metal alloy coatings. *Surf Coat Tech* 2008; 202: 4793–4809.
2. Fantozzi D, Matikainen V, Uusitalo M, et al. Chlorine-induced high temperature corrosion of Inconel 625 sprayed coatings deposited with different thermal spray techniques. *Surf Coat Tech* 2017; 318: 233–243.
3. Chen TC, Chou CC, Yung TY, et al. A comparative study on the tribological behavior of various thermally sprayed Inconel 625 coatings in a saline solution and deionized water. *Surf Coat Tech* 2020; 385.
4. Oladijo OP, Collieus LL, Obadele BA, et al. Correlation between residual stresses and the tribological behaviour of Inconel 625 coatings. *Surf Coat Tech* 2021; 419. doi:10.1016/j.surfcoat.2021.127288
5. Boudi A, Hashmi MSJ and Yilbas BS. Tensile properties of HVOF sprayed Inconel 625 coatings subjected aqueous corrosion. *Ind Lubr Tribol* 2006; 58: 45–49.
6. Goyal DK, Singh H and Kumar H. An overview of slurry erosion control by the application of high velocity oxy fuel sprayed coatings. *P I Mech Eng J-J-Eng* 2011; 225: 1092–1105.
7. Ghadami F and Aghdam ASR. Improvement of high velocity oxy-fuel spray coatings by thermal post treatments: a critical review. *Thin Solid Films* 2019; 678: 42–52.
8. Lindner T, Löbel M, Hunger R, et al. Boriding of HVOF-sprayed Inconel 625 coatings. *Surf Coat Tech* 2020; 404.
9. Liu Z, Cabrero J, Niang S, et al. Improving corrosion and wear performance of HVOF-sprayed inconel 625 and WC-Inconel 625 coatings by high power diode laser treatments. *Surf Coat Tech* 2007; 201: 7149–7158.
10. Mindivan F and Mindivan H. Surface properties and tribocorrosion behaviour of a thermal sprayed martensitic stainless steel coating after pulsed plasma nitriding process. *Adv Mat Proc Tech* 2016; 2: 514–526.
11. Mindivan H. Investigating tribological characteristics of HVOF sprayed AISI 316 stainless steel coating by pulsed plasma nitriding. *Iop Conf Series: Mater Sci Eng* 2018; 295: 1–7.
12. Musil J, Vlcek J and Ruzicka M. Recent progress in plasma nitriding. *Vacuum* 2000; 59: 940–951.
13. Borowski T, Brojanowska A, Kost M, et al. Modifying the properties of the Inconel 625 nickel alloy by glow discharge assisted nitriding. *Vacuum* 2009; 83:1489–1493.

14. Podgornik B, Vizintin J and Leskovsek V. Tribological properties of plasma and pulse plasma nitrided AISI 4140 steel. *Surf Coat Tech* 1998; 108–109: 454–460.
15. Podgornik B and Vizintin J. Wear resistance of pulse plasma nitrided AISI 4140 and A355 steels. *Mat Sci Eng A* 2001; 315: 28–34.
16. Varela LB, Ordoñez M F. C., Pinedo CE, et al. Micro-abrasive wear study of a low-temperature plasma nitrided Inconel 625 superalloy. *Tribol – Mater Surf Interfaces* 2021.
17. Ponthiaux P, Wenger F, Drees D, et al. Electrochemical techniques for studying tribocorrosion processes. *Wear* 2004; 256: 459–468.
18. Papageorgiou N, Bonin AV and Espallargas N. Tribocorrosion mechanisms of NiCrMo-625 alloy: an electrochemical modeling approach. *Tribol Int* 2014; 73: 177–186.
19. Park G, Bae G, Moon K, et al. Effect of plasma nitriding and nitrocarburizing on HVOF-sprayed stainless steel coatings. *J Therm Spray Techn* 2013; 22: 1366–1373.
20. Espallargas N and Mischler S. Dry wear and tribocorrosion mechanisms of pulsed plasma nitrided Ni–Cr alloy. *Wear* 2011; 270:464–471.
21. Zhang Y, Wang Q, Chen G, et al. Mechanical, tribological and corrosion physiognomies of CNT-Al metal matrix composite (MMC) coatings deposited by cold gas dynamic spray (CGDS) process. *Surf Coat Tech* 2020; 403.
22. Boztepe E, Alves AC, Ariza E, et al. A comparative investigation of the corrosion and tribocorrosion behaviour of nitrocarburized, gas nitrided, fluidized-bed nitrided, and plasma nitride plastic mould steel. *Surf Coat Tech* 2018; 334: 116–123.
23. Neville A and Hodgkiess T. Towards novel ceramic base coatings for corrosive wear applications. *Brit Corros J* 1999; 34: 262–266.
24. Totolin V, Pejaković V, Csanyi T, et al. Surface engineering of Ti6Al4 V surfaces for enhanced tribocorrosion performance in artificial seawater. *Mater Design* 2016; 104: 10–18.